Appl. Phys. A (2014) 116:1905–1913
DOI 10.1007/s00339-014-8351-1

Applied Physics A
Materials Science & Processing

On the phase formation of titanium oxide thin films deposited by reactive DC magnetron sputtering: influence of oxygen partial pressure and nitrogen doping

Ramanathaswamy Pandian · Gomathi Natarajan · S. Rajagopalan · M. Kamruddin · A. K. Tyagi

Received: 22 October 2013 / Accepted: 25 February 2014 / Published online: 16 March 2014

Abstract This work describes about the control on phase formation in titanium oxide thin films deposited by reactive dc magnetron sputtering. Various phases of titanium oxide thin films were deposited by controlling the oxygen partial pressure during the sputtering process. By adding nitrogen gas to sputter gas mixture of oxygen and argon, the oxygen partial pressure was decreased further below the usual critical value, below and above which the sputtering yields metallic and oxide films, respectively. Furthermore, nitrogen addition eliminated the typical hysteretic behaviour between the flow rate and oxygen partial pressure, and significantly influenced the sputter rate. On increasing the oxygen partial pressure, the ratio between anatase and rutile fraction and grain size increases. The fracture cross-sectional scanning electron microscopy together with the complementary information from X-ray diffraction and micro-Raman investigations revealed the evolution and spatial distribution of the anatase and rutile phases. Both the energy delivered to the growing film and oxygen vacancy concentrations are correlated with the formation of various phases upon varying the oxygen partial pressure.

1 Introduction

Titanium oxide, a versatile material, has been widely investigated in powder or thin film form due to its wide variety of applications including photocatalysis [1, 2], anti-corrosion [3], light- and gas-sensors [4, 5], electronic (memory) switching [6, 7], electrochromics [8, 9], pigments, and charge separating devices [10, 11] (e.g. de-synthesized solar cells). The demand for tailoring the material properties to meet specific application requirements and miniaturization of devices attracted much attention to the fabrication of titanium oxide mostly in the form of thin films and nanostructures. As far as the titanium oxide thin films are considered, most of the applications in general are microstructure (crystallographic phase) dependent. Anatase phase of titanium oxide, for instance, is known to exhibit pronounced photocatalytic [12–14], photoluminescence [15] and super-hydrophilic activity [16, 17]. Rutile finds applications in optical coatings due to its high refractive index [18–20] and also shows interesting dielectric properties [18, 21, 22]. Therefore, having control on the crystallographic phase of the film is vital for the targeted applications which are phase dependent.

Though the microstructural modifications are possible during or after the film deposition, the former is always preferred. Numerous techniques including sol–gel, hydrothermal, direct oxidation, chemical vapour deposition, physical vapour deposition, electrodeposition, sonochemical and microwave, as summarized in Ref. [23], have been explored to synthesize titanium oxide films. Among them, however, sputter deposition is preferable for fabricating thin films with large area thickness uniformity, good reproducibility and large-scale industrial production. Besides, this technique offers the possibility of altering the film properties during the deposition by controlling one or more sputtering parameter(s) [24, 25]. For instance, sputter deposition of crystalline thin films is possible at room temperatures. In this case, the energy for crystallization is delivered via bombardment of energetic particles to the growing film. This, therefore, facilitates the usage of heat-

R. Pandian (✉) · G. Natarajan · S. Rajagopalan · M. Kamruddin · A. K. Tyagi
Surface and Nanoscience Division, Materials Science Group, Indira Gandhi Center for Atomic Research, Kalpakkam 603102, India
e-mail: rpandian@igcar.gov.in

sensitive substrates like polymers; otherwise conventionally the substrates are heated to high temperatures during or after the film deposition. In order to understand the correlation between the crystallographic phase and deposition conditions (or parameters) in sputtered titanium oxide thin films, some efforts have been previously made. The phase formation as a function of total pressure [26–29], film thickness [30], magnetic field strength [31], magnetron configuration [32, 33], nature of sputtering gas [34], energies of ions or particles bombarding the substrate [21, 35, 36] and substrate temperature [29, 35, 37] has been attempted. However, a complete understanding on various critical factors influencing the phase formation during the film growth has not yet been realized.

In this article, we discuss about the formation of various phases of titanium oxide thin films influenced by the sputtering gas atmosphere, particularly the effect of oxygen partial pressure and addition of nitrogen gas during the sputtering process. In principle, there is a critical value of oxygen partial pressure which determines the deposition of compound or metallic films in a reactive sputtering process. The oxygen partial pressure, in fact, could be varied with the oxygen flow, and above the critical value of oxygen partial pressure, the sputtering process switches from metallic to compound mode. In this work, we also demonstrate the possibility of pushing the limit associated with oxygen partial pressure further down by adding nitrogen during the sputtering process. With the extended window of sputtering process of oxide film regarding oxygen partial pressure, we demonstrate the growth of titanium oxide thin films (on silicon substrates without any intentional heating) with various phases from anatase-rich to rutile-rich via mixture of both.

2 Experimental procedure

Titanium oxide thin films were deposited onto well-cleaned silicon substrates using reactive DC magnetron sputtering technique with a titanium target of 99.99 % purity. The size of the sputtering target was 76.2 mm, and the target to substrate spacing was maintained around 55 mm. The deposition was carried out in a mixed gas atmosphere containing argon, oxygen and nitrogen (in some cases) at a constant sputtering current of 0.9 A. The substrates were not intentionally heated, but it was observed that the temperature of the substrate surface reaches as high as 160 °C for the deposition time of 1 h. Oxygen partial pressure in the sputtering chamber was varied by controlling the oxygen and/or nitrogen flow, and the argon flow was adjusted accordingly to maintain a constant working pressure of 8×10^{-3} mbar. In order to achieve a constant film thickness of about 200 nm, the time of deposition was adjusted according to the variations in sputtering rate at different oxygen partial pressures. The summary of the experimental specifications are given in Table 1. The sputtered films were characterized by various techniques to study the correlation between the oxygen partial pressure and phase formation. The surface morphology and microstructure of the films were analysed by field emission scanning electron microscopy (FE-SEM) with ZEISS SUPRA 55 microscope. Formation of different crystalline phases was studied by grazing incidence X-ray diffraction (GI-XRD) technique with Bruker D8 discover diffractometer (using Cu K_α radiation with $\lambda \sim 0.15418$ nm). Micro-Raman scattering measurements were performed by Renishaw's inVia system with 514.5-nm line of Ar^+ laser excitation using 50× objective lens and 1,800 groves/mm grating assisted with thermoelectric cooled CCD detector in the backscattering configuration for in-depth structural elucidation of the specimens. The chemical composition of the films was determined by X-ray photoelectron spectroscopy (XPS) with SPECS spectrometer (using Al K_α source with 1,486.74 eV energy), and further details about these measurements will be published elsewhere.

Table 1 Summary of experimental conditions for the sputtering of various titanium oxide films

Sample name	Oxygen partial pressure (mPa)	Oxygen flow (sccm)	Nitrogen flow (sccm)
A	80	7.6	0
B	50	4.9	0
C	30	3.5	4
D	10	2.0	4

3 Results and discussion

Figure 1 shows the hysteretic behaviour, between oxygen partial pressure and oxygen flow, of the sputtering process of metallic titanium target in oxygen atmosphere (Fig. 1a), and in case of addition of 4 sccm nitrogen (Fig. 1b). The hysteresis shown in Fig. 1a resembles a typical reactive sputtering process of a metallic target. On increasing the oxygen flow (forward sweep), the process switches from metallic to oxidic (or compound) mode through a sharp transition. Up to a certain value of oxygen flow, oxygen is adsorbed on the target surface by a gettering process and the sputtered films are mainly metallic. When the flow crosses the critical value, oxidic films are obtained due to target poisoning. As marked in the hysteresis curve (Fig. 1a) with larger dark circles, two thin film specimens, named *A* and *B*, were sputtered in oxygen ambient. Specimen *A* was deposited deep in the oxidic mode at 80 mPa oxygen partial pressure, and *B* was deposited during the

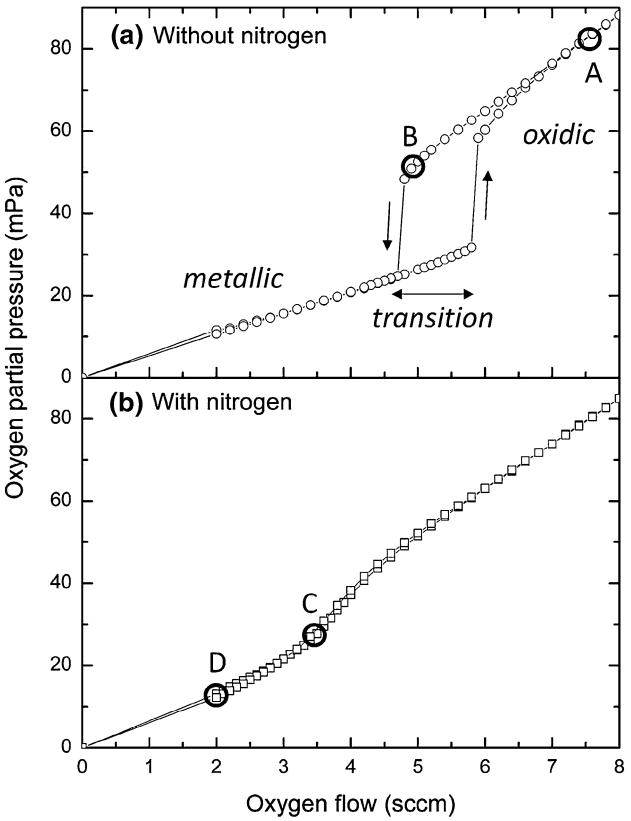

Fig. 1 Oxygen flow versus oxygen partial pressure hysteresis of titanium sputtering **a** in pure oxygen atmosphere and **b** with 4 sccm nitrogen flow

reverse sweep at 50 mPa oxygen partial pressure (in the transition regime) just before the sputtering falls into the metallic mode.

Figure 1b shows the effect of incorporation of 4 sccm nitrogen during the sputtering process. The typical hysteretic behaviour vanishes, and a smooth transition from metallic mode to oxidic mode of sputtering occurs. Moreover, the sputtering rate is increased up to 4 times compared with that in pure oxygen ambient (see the curve corresponds to the right *Y*-axis of Fig. 2). This is related to the higher erosion rate of nitride compared with the oxide formed on the target surface, which is predominantly covered by the nitride. A strong influence of nitrogen inclusion on the oxidic sputtering of other metals is reported in Ref. [38]. As seen in Fig. 1b, nitrogen addition facilitates deposition of titanium oxide at reduced oxygen partial pressures, which otherwise would lead to the deposition of metallic films. In the presence of nitrogen, specimens *C* and *D* were deposited at 30 and 10 mPa oxygen partial pressure, respectively, as marked in Fig. 1b with larger black circles. Note that the nitrogen flow was kept constant at 4 sccm and the oxygen flow was varied, which was 3.5 and 2 sccm for depositing specimen *C* and specimen *D*, respectively.

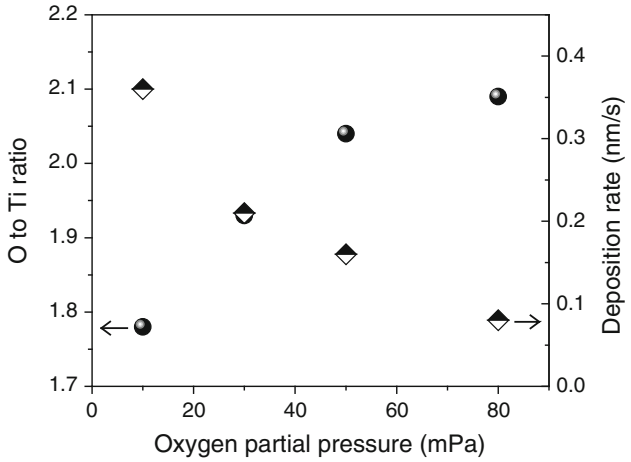

Fig. 2 Influence of oxygen partial pressure on the O/Ti ratio (in *left Y-axis*) and deposition rate (in *right Y-axis*)

The composition stoichiometry of the films was analysed by XPS using the $Ti2p_1$ and O1s core level spectra. It was found that O/Ti ratio increases with the oxygen partial pressure as seen in Fig. 2 (curve corresponds to left *Y*-axis). This means that the compound formation is limited at low oxygen partial pressures, whereas the film is saturated with oxygen at high oxygen partial pressures. This further indicates that the oxygen vacancy concentration in the films increases with the decrease in the oxygen partial pressure. In the case of nitrogen addition, in specimen *C* and *D*, the amount of nitrogen incorporated is about 1.2 and 2.4 atomic percentage, respectively. It is interesting to note that nitrogen incorporation in these sputtered films is very low compared with oxygen although oxygen and nitrogen flows were almost comparable (as in the case of specimen *C*, for example). This is attributed to the replacement of metal nitride by oxide due to higher reactivity of the later [39].

The influence of oxygen partial pressure on the microstructure and surface morphology of the films was investigated by FE-SEM, and the corresponding secondary electron images are shown in Fig. 3. Variations in the microstructure and surface morphology are shown in the fracture cross-sectional (right) and plan-view (left) images, respectively. Specimen *A*, deposited at 80 mPa oxygen partial pressure, consists of columnar grains aligned vertically to the substrate plane (see Fig. 3a). The film surface appears to be rough and consists of faceted grains resembling an array of different polygons. A careful observation revealed the presence of small fraction (<20 %) of fine grains composing a layer underneath the columnar grains at the film–substrate interface. This indicates that the film consists of two distinct grain types. In specimen *B*, for an oxygen partial pressure of 50 mPa, the columnar growth has considerably diminished. Therefore, there is a reduction in

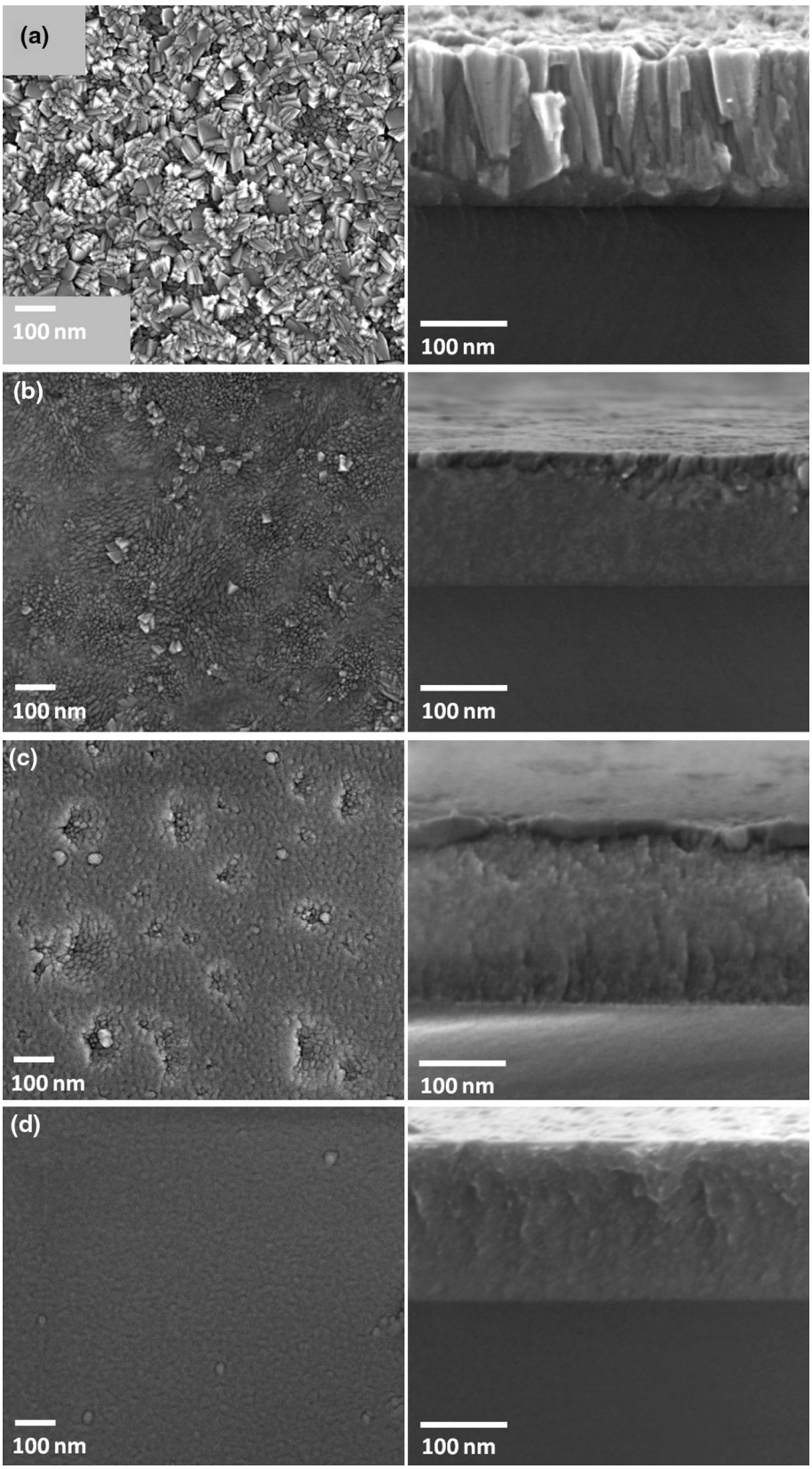

Fig. 3 Plan-view (*left*) and cross-sectional (*right*) FE-SEM images of titanium oxide thin films sputtered at various oxygen partial pressures; **a** 80 mPa, **b** 50 mPa, **c** 30 mPa and **d** 10 mPa

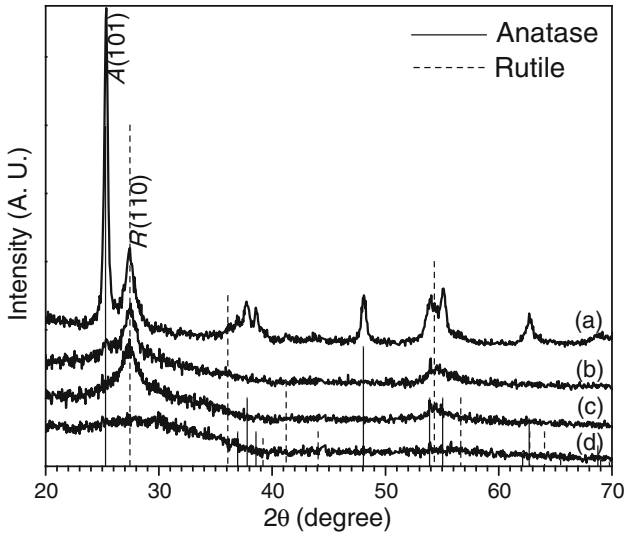

Fig. 4 Grazing incidence XRD patterns of titanium oxide thin films sputtered at various oxygen partial pressures; **a** 80 mPa, **b** 50 mPa, **c** 30 mPa and **d** 10 mPa

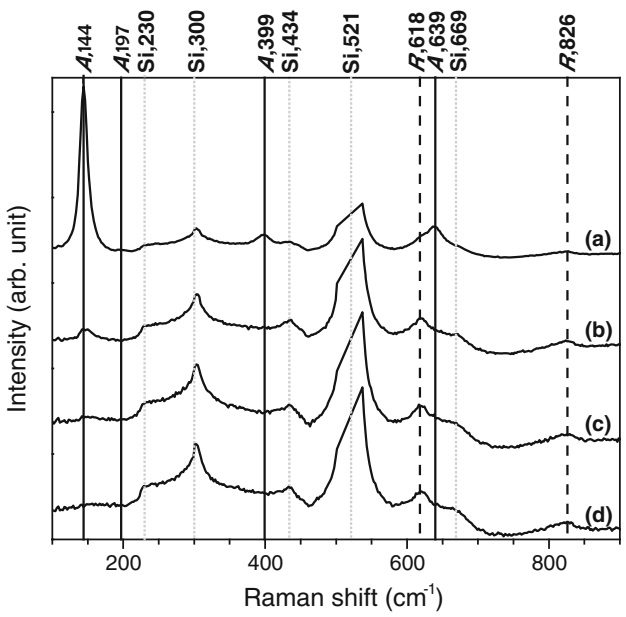

Fig. 5 Micro-Raman spectra of titanium oxide thin films sputtered at various oxygen partial pressures; **a** 80 mPa, **b** 50 mPa, **c** 30 mPa and **d** 10 mPa

the fraction of coarse grains down to ~30 %, and the fine grains occupy the remaining volume of the film (see Fig. 3b). The vertical dimension of the coarse grains is found to be reduced drastically compared with the previous case. Though the cross-sectional image of the specimen shows a bi-layer-like structure, the plan-view image recorded at relatively low magnification reveals that the surface is not fully covered by the coarse grains. Instead, the elongated coarse grains appear as large clusters in the background of fine grains. The microstructure of specimen *C*, deposited at 30 mPa oxygen partial pressure with nitrogen inclusion, is shown in Fig. 3c. The plan-view image shows the size and distribution of the clusters of coarse grains in the background of fine grains. The cluster size and density have significantly reduced in comparison with specimen *B*. Major volume fraction of the specimen (about 90 %) and its surface is occupied by the fine grains. The cross-sectional image shows that the coarse grain clusters at the film surface. While decreasing the oxygen partial pressure further down to 10 mPa (at a nitrogen flow of 4 sccm and oxygen flow of 2 sccm, as in the case of specimen *D*), the columnar grains entirely disappear and the film microstructure is dominated by the fine grains (see Fig. 3d). The film appears to be homogeneous with relatively smooth surface as there is no contribution from the coarse grains.

The specimens were further analysed by grazing incidence XRD with 0.5° angle of incidence to investigate on the crystallinity and phase, and the results are shown in Fig. 4. The diffraction peaks corresponding to various crystal planes of anatase and rutile phases are indicated by solid and dashed vertical lines, respectively, in the figure. The signature peak of anatase and rutile emerges at 2θ values of 25.3° and 27.45°, respectively [40]. According to Fig. 4a, specimen *A* is predominantly anatase with some amount of rutile phase. On the other hand, specimen *D* shows no pronounced diffraction peak, and this therefore indicates amorphous phase or very small crystallites. However, the overall conclusion drawn from the XRD analysis is that the ratio between anatase and rutile fraction and the grain size increases with the oxygen partial pressure. The grain growth in anatase phase with the increase in oxygen partial pressure is well distinguished than that in rutile. Correlating the XRD results to the corresponding SEM images indicates that the faceted coarse grains are anatase and granular fine grains are rutile. This correlation fits also well with the previous results in literature [41–45].

The specimens were analysed by micro-Raman technique in order to clarify further on the crystallographic phase formation. Since the micro-Raman technique, in principle, is sensitive to the presence of short-range order in materials, comprehensive information on the microstructure could be derived. Particularly specimen *D*, which appears to be X-ray amorphous, is expected to consist of fine rutile crystallites if the assumption that the fine grains appear in SEM image are rutile is valid. The Raman spectra for the specimens are presented in Fig. 5, where the Raman peaks for anatase and rutile phase are marked as *A* and *R*, respectively, along with their peak positions [46–50] and the substrate peaks are marked as *Si* [51–53]. Specimen *A* shows a strong anatase peak at ~144 cm^{-1} that belongs to E_g mode of vibration. This peak is in fact related to O–

Ti–O bending type vibration predominantly. Additional peaks for anatase phase appear at ~197, 399 and 639 cm^{-1} belong to E_g, B_{1g} and E_g mode of vibration, respectively. The rutile peak appears at ~612 cm^{-1} belongs to A_{1g} mode, and it is related to Ti–O stretching-type vibration predominantly. Another rutile peak appears at ~826 cm^{-1} belongs to B_{2g} mode, and it is related to O–Ti–O stretching (i.e. both oxygen atoms move simultaneously towards or away from central Ti) [54]. Raman spectra for the specimens *A* to *C* reveal that the anatase peak intensity at ~144 cm^{-1} decreases with oxygen partial pressure, and this inference agrees well with the XRD results. Raman spectrum of specimen *D* does not show any anatase peak; however, the presence of rutile phase could be identified by the peaks at ~612 and ~826 cm^{-1}. It should be noted that the XRD pattern of this specimen did not show any crystalline peak(s) except a broad amorphous hump (see Fig. 4d), and this is related to the technical limitation of the X-ray method in distinguishing very short-range ordered crystalline phases from the amorphous content [55, 56].

Therefore, intercorrelating the results from the SEM, XRD and micro-Raman techniques, it could conclusively be stated that the finer (spherical) and coarser (columnar) grains are mainly composed of rutile and anatase, respectively (see Figs. 3d, 4d, 5d). In order to better understand about the spatial distribution of the anatase and rutile grains along the thickness of the film, angle-dependent grazing incidence XRD was performed with a sample of 300 nm deposited in the oxidic mode, i.e. with deposition conditions similar to sample A. The incidence angle was varied from 0.3 to 1.5° (corresponds to probing depths of approximately 60–300 nm), and the results are shown in Fig. 6. There is no rutile peak observed for an inclination angle of 0.3°, a less intense peak appeared for 0.5°, the peak intensity then increased for 1° and remained the same for angles above 1.5°. The observation confirms the presence of rutile phase at the film–substrate interface and buried under the anatase phase that is present in the film surface. A similar observation is also reported in ref. [30]. The shift in the peak position of anatase phase may be related to the difference in the strain and a possible difference in grain size at the film surface and deeper into the film.

The cause of the formation of bi-layer like structure in our samples is not yet fully understood, although it was reported in other studies [30]. However, anatase grain growth is speculated to be initiated by the (unintentional) heating of the substrate during the deposition, and the substrate heating in case of longer deposition times must be considered. Our recent measurements showed that the deposition conditions similar to that adopted for sample A resulted in heating up of the substrate surface as high as

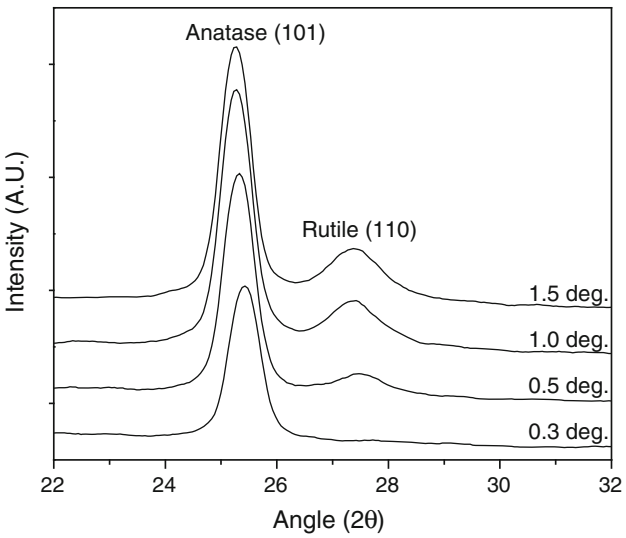

Fig. 6 Angle-dependant grazing incidence XRD patterns of a titanium oxide thin film sputtered in oxidic mode

160 °C for the sputtering time of 1 h. The grain growth will then be possible due to the substrate heating along with the kinetic energies of the particle bombardments. The authors consider that the following might be the reason for the presence of anatase above the rutile. At the beginning of the film growth, oxygen vacancy defects are created due to particle bombardments and preferential removal of oxygen from the stoichiometric titanium oxide [57]. The oxygen vacancies generally favour to rutile growth by acting as nucleation sites for the growth of rutile nuclei [58, 59]. In later stages of the deposition, the vacancy concentration might be reduced due to the substrate heating [60] favouring the anatase nucleation. From thermodynamic point of view, the rapid growth of anatase could also be due to its lower surface free energy (though the rutile has a slightly lower Gibbs free energy) [61]. The nucleation of anatase does not necessarily mean the rutile to anatase transformation, but it could be originated from the amorphous fraction that exists with the rutile nanocrystals [62]. The presence of the amorphous fraction could be realized from the broad diffraction peaks seen in Fig. 4c, d, and is expected to be located at the grain boundaries [63].

It is shown, in this work, that adding nitrogen during sputtering has the following effects: (a) reduction in the lower limit of oxygen partial pressure for the deposition of compound films in oxidic mode, (b) an increase in the sputter rate compared to argon–oxygen atmosphere and (c) deposition of rutile or rutile-rich mixed phases with very low (<2.4 atomic %) nitrogen incorporation in the films without intentional substrate heating. Apart from that, higher oxygen partial pressures (without nitrogen incorporation) favour the formation of anatase phase, while the lower oxygen partial pressures (with nitrogen incorporation) are in favour of the

rutile growth. There are several concepts proposed in literature to explain the correlation between the crystallographic phase formation in the deposited films and sputtering parameters. However, the most convincing explanation is based on the total energy delivered to the growing film. The total energy is attributed to the crystallization of the film through the migration of ad-atoms on the substrate [42, 64, 65]. The crystallization is enhanced by increasing the total energy [36, 66]. There are reports in literature on the enhancement crystal growth as a result of ion bombardment or high-energy neutral particle bombardment during deposition [67, 68]. The total energy, in fact, includes the contributions from the following: (1) intentional substrate heating, (2) energy from the bombarding species, (3) the heat coming from the target and the plasma (resulting unintentional heating of the substrate) and (4) energy due to the exothermic chemical reaction during the compound formation. Moreover, the rate of deposition is found to be a crucial parameter in determining the phase formation. Lower deposition rates (means longer deposition times) yield higher crystallinity, whereas higher rates lead to lower crystallinity or sometimes amorphous phase. It is to be noted that with sufficiently longer deposition times, the unintentional heating of the substrate becomes significant in determining the crystallinity of the film. In addition to the effect of the lower deposition rate, the reason for higher crystallinity observed in our samples might be the stoichiometric factor due to higher oxygen partial pressure and the (significant) substrate heating due to longer deposition time. The possibilities of formation of various phases (including the amorphous phase) with respect to the energy of the particles bombarding on the substrate at various substrate temperatures are reported in Ref. [21].

The deposition rate, in our case, significantly decreases as the oxygen partial pressure increases. As mentioned earlier in the report, upon increasing the oxygen partial pressure from 10 to 80 mPa, the deposition rate decreased by 4 times (see Fig. 2). This, therefore, can directly be related to the decrease in the sputtering yield due to the increase in surface coverage of the target by compound formation [69]. For a constant sputtering current of 0.9 A, the sputtering voltage increases from $\sim$360 to 450 V if oxygen partial pressure is increased from 10 to 80 mPa. This is expected to be related to the growth of insulating Ti–O compound on the target surface at higher oxygen partial pressures [70]. Therefore, the effective voltage contributed to the acceleration of charged particles is likely to be lower compared with that at lower oxygen partial pressures. This means that the energy delivered to the sputtered particles is inadequate at higher oxygen partial pressures to grow rutile phase while at lower oxygen partial pressures, the sputtered particles, with high sputtering yield, arrive at the substrate with sufficient energy to grow rutile phase.

Although the phase formation is described in terms of oxygen partial pressure and energy transfer, an understanding from the point of view of oxygen vacancy creation and the consequences on the film growth and phase formation upon nitrogen incorporation during sputtering is also necessary. The following discussion deals about the role of incorporated nitrogen on the phase formation. The influence of impurity and growth (or deposition) atmosphere on the microstructural transformations, particularly from anatase to rutile, could be explained in terms of defects generated in titanium oxide film. The defects could be either interstitial titanium ions or oxygen vacancies [71–73]. The ions are, in principle, expected to inhibit the transformation by hindering the atomic diffusion, whereas the vacancies tend to promote the transformation by rupturing of two Ti–O bonds out of six and forming new bonds. In general, substitution of oxygen sites by nitrogen atoms is not likely to occur due to the larger ionic radius of nitrogen (1.71 Å) compared with that of oxygen (1.40 Å). Instead, two nitrogen atoms could substitute three oxygen atoms by maintaining the chemical state of Ti (Ti^{4+}), and this eventually results in the formation of one oxygen vacancy [74]. Since the rutile phase is capable of accepting large number of defects than anatase, its formation is favoured at conditions promoting large number of defects/vacancies for instance at lower oxygen partial pressures [75, 76]. Moreover, it has been noticed that oxygen deficiency in the film decreases while increasing the oxygen concentration in the sputtering environment [77]. This means that at higher oxygen partial pressures, as the formation of the vacancy-related defects are less likely, the anatase phase formation might be favoured. Hence, by considering both the above-mentioned concepts, it is believed that the *energy transfer* can be predominantly responsible at higher oxygen partial pressures, whereas the *energy transfer* as well as *oxygen vacancy* is responsible at lower oxygen partial pressures for the observed phases in the sputtered films.

4 Conclusions

Titanium oxide thin films with various combinations of anatase and rutile phases were deposited on silicon substrates by reactive DC magnetron sputtering using titanium target in the atmosphere of argon, oxygen and nitrogen gas mixture. Addition of nitrogen extended the window of oxygen partial pressure that could be used to deposit the oxide thin films with a small amount of nitrogen incorporation (<2.4 at.%). Upon increasing the oxygen partial pressure, various phases of titanium dioxide films from rutile to anatase-rich via a mixed phase were deposited. At lower oxygen partial pressures, the films were predominantly rutile

with fine grains, whereas at higher oxygen partial pressures, coarse-grained anatase phase dominated in the film. The energy delivered to the growing film and nitrogen incorporation during sputtering are attributed to the formation of various phases with respect to oxygen partial pressure.

Acknowledgments The authors would like to thank and appreciate Dr. S. Dhara, Surface and Nanoscience Division, Indira Gandhi Center for Atomic Research, Kalpakkam, India, for offering the micro-Raman facility. Likewise, Mr. Nanda Gopala Krishna Dhaipule and Dr. U. Kamachi Mudali, Corrosion Science and Technology Group, Indira Gandhi Centre for Atomic Research, Kalpakkam, India, for the XPS measurements.

References

1. A. Fujishima, T.N. Rao, D.A. Tryk, J. Photochem. Photobiol. C **1**, 1 (2000)
2. D.M. Blake, P.-C. Maness, Z. Huang, E.J. Wolfrum, J. Huang, W.A. Jacoby, Sep. Purif. Methods **28**, 1 (1999)
3. Z. Ahmad, M. Ahsan, Anti-Corros. Methods Mater. **56**, 187 (2009)
4. W.O. Williamson, Nature **140**, 238 (1937)
5. Y. Komem, G. Ankonina, A. Rothschild, J.S. Im, U.J. Chung, Phys. Scr. **T129**, 157 (2007)
6. F. Argall, Solid State Electron. **11**, 535 (1968)
7. G. Dearnaley, A.M. Stoneham, D.V. Morgan, Rep. Prog. Phys. **33**, 1129 (1970)
8. M. Ottaviani, S. Panero, S. Morzilli, B. Scrosati, M. Lazzari, Solid State Ion. **20**, 197 (1986)
9. T. Ohsuku, T. Hirai, Electrochim. Acta **27**, 1263 (1982)
10. Y. Tachibana, J.E. Moser, M. Grätzel, D.R. Klug, J.R. Durrant, J. Phys. Chem. **100**, 20056 (1996)
11. I. Chung, B. Lee, J. He, R.R.H. Chang, M.G. Kanatzidis, Nature **485**, 486 (2012)
12. J. Zhang, T. Ayusawa, M. Minagawa, K. Kinugawa, H. Yamashita, M. Matsuoka, M. Anpo, J. Catal. **198**, 1 (2001)
13. J. Zhang, Y. Hu, M. Matsuoka, H. Yamashita, M. Minagawa, H. Hidaka, M. Anpo, J. Phys. Chem. B **105**, 8395 (2001)
14. D.R. Park, J. Zhang, K. Ikeue, H. Yamashita, M. Anpo, J. Catal. **185**, 114 (1999)
15. Y. Jin, G. Li, Y. Zhang, Y. Zhang, L. Zhang, J. Phys. Condens. Matter **13**, L913 (2001)
16. K. Takagi, T. Makimoto, H. Hiraiwa, T. Negishin, J. Vac. Sci. Technol. A **19**, 2931 (2001)
17. P. Zeman, S. Takabayashi, J. Vac. Sci. Technol. A **20**, 388 (2002)
18. K. Okimura, Surf. Coat. Technol. **135**, 286 (2001)
19. H. Tang, K. Prasad, R. Sanjinès, P.E. Schmid, F. Lévy, J. Appl. Phys. **75**, 2042 (1994)
20. G. Hass, Vacuum **2**, 331 (1952)
21. P. Loebl, M. Huppertz, D. Mergel, d. Thin Solid Films **251**, 72 (1994)
22. J.V. Grahn, M. Lindner, E. Fredriksson, J. Vac. Sci. Technol. A **16**, 2495 (1998)
23. X. Chen, S. Mao, Chem. Rev. **107**, 2891 (2007)
24. L.J. Meng, M.P. dos Santos, Thin Solid Films **226**, 22 (1993)
25. R. Knizikevičius, ISSN 1392–1320 Mater. Sci. (Medžg.) **16**, 202 (2010)
26. P. Zeman, S. Takabayashi, Surf. Coat. Technol. **153**, 93 (2002)
27. M. Yamagishi, S. Kuriki, P.K. Song, Y. Shigesato, Thin Solid Films **442**, 227 (2003)
28. N. Martin, A.M.E. Santo, R. Sanjines, F. Levy, Surf. Coat. Technol. **138**, 77 (2001)
29. P. Zeman, S. Takabayashi, Thin Solid Films **433**, 57 (2003)
30. R. Kuzel, L. Nichtova, D. Herman, J. Sicha, J. Musil, Z. Kristallogr. **Suppl. 26**, 241 (2007)
31. P.K. Song, Y. Irie, S. Ohno, Y. Sato, Y. Shigesato, Jpn. J. Appl. Phys. **43**, L442 (2004)
32. K. Okimura, Surf. Coat. Technol. **135**, 286 (2001)
33. O. Zywitzki, T. Modes, H. Sahm, P. Frach, K. Goedicke, D. Glöß, Surf. Coat. Technol. **180–181**, 538 (2004)
34. P.K. Song, Y. Irie, Y. Sato, Y. Shigesato, Jpn. J. Appl. Phys. **43**, L358 (2004)
35. Y. Leprince-Wang, D. Souche, K. Yu-Zhang, S. Fisson, G. Vuye, J. Rivory, Thin Solid Films **359**, 171 (2000)
36. J. Musil, J. Sicha, D. Herman, R. Cerstvy, J. Vac. Sci. Technol. A **25**, 666 (2007)
37. R. Kuzel, L. Nichtova, Z. Matej, J. Sicha, J. Musil, Z. Kristallogr. **Suppl. 27**, 287 (2008)
38. D. Severin, O. Kappertz, T. Kubart, T. Nyberg, S. Berg, A. Pflug, M. Siemers, M. Wuttig, Appl. Phys. Lett. **88**, 161504 (2006)
39. D. Severin, K. Sarakinos, O. Kappertz, A. Pflug, M. Wuttig, J. Appl. Phys. **103**, 083306 (2008)
40. International Centre for Diffraction Data, PDF ID No. 21-1272 and 21-1276
41. P. Zeman, S. Takabayashi, Surf. Coat. Technol. **153**, 93 (2002)
42. J. Musil, D. Herman, J. Sicha, J. Vac. Sci. Technol. A **24**, 521 (2006)
43. J. Musil, J. Sicha, D. Herman, R. Cerstvy, J. Vac. Sci. Technol. A **25**, 666 (2007)
44. K. Okimura, Surf. Coat. Technol. **135**, 286 (2001)
45. S. Takeda, S. Suzuki, H. Odaka, H. Hosono, Thin Solid Films **392**, 338 (2001)
46. L.D. Arsov, C. Kormann, W. Plieth, J. Raman Spectrosc. **22**, 573 (1991)
47. H. Chang, P.J. Huang, J. Raman Spectrosc. **29**, 97 (1998)
48. D.C. Cronemeyer, Phys. Rev. **87**, 876 (1952)
49. S.P.S. Porto, P.A. Fleury, T.C. Damen, Phys. Rev. **154**, 522 (1967)
50. V. Swamy, A. Kuznetsov, L.S. Dubrovinsky, R.A. Caruso, D.G. Shchukin, B.C. Muddle, Phys. Rev. B **71**, 184302 (2005)
51. J.H. Parker, D.W. Feldman, M. Ashkin, Phys. Rev. **155**, 712 (1967)
52. K.J. Kingma, R.J. Hemley, Am. Mineral. **79**, 269 (1994)
53. I. De Wolf, Semicond. Sci. Technol. **11**, 139 (1996)
54. D. Krishnamurti, Proc. Indian Acad. Sci. Sect. A **55**, 290 (1962)
55. T. Asanuma, T. Matsutani, C. Liu, T. Mihara, M. Kiuchi, J. Appl. Phys. **95**, 6011 (2004)
56. D. Mardare, Mater. Sci. Eng. B **95**, 83 (2002)
57. J.T. Mayer, U. Diebold, T.E. Madey, E. Garfunkel, J. Electron Spectrosc. Relat. Phenom. **1–11**, 73 (1995)
58. C. Rath, P. Mohanty, A.C. Pandey, N.C. Mishra, J. Phys. D Appl. Phys. **42**, 205101 (2009)
59. R.D. Shannon, J. Appl. Phys. **35**, 3414 (1964)
60. H. Tomaszewski, H. Poelman, D. Depla, D. Poelman, R. De Gryse, L. Fiermans, M.F. Reyniers, G. Heynderickx, G.B. Marin, Vacuum **31–38**, 68 (2003)
61. D.A.D. Hanaor, C.C. Sorrell, J. Mater. Sci. **46**, 855 (2011)
62. H. Zhang, J.F. Banfield, Chem. Mater. **14**, 4145 (2002)
63. B. Choudhury, A. Choudhury, Int. Nano Lett. **3**, 55 (2013)
64. P. Zeman, S. Takabayashi, Surf. Coat. Technol. **153**, 93 (2002)
65. K. Okimura, A. Shibata, N. Maeda, K. Tachibana, Y. Noguchi, K. Tsuchida, Jpn. J. Appl. Phys. **34**(4950), 90 (1995)
66. J. Musil, D. Herman, J. Sicha, J. Vac. Sci. Technol. A **24**, 521 (2006)
67. J.E. Greene, S.A. Barnett, J. Vac. Sci. Technol. **21**, 285 (1982)
68. I. Petrov, L. Hultman, U. Helmerson, J.E. Sundgren, J.E. Greene, Thin Solid Films **169**, 299 (1989)
69. T. Abe, T. Yamashina, Thin Solid Films **38**, 271 (1976)

70. D. Wicaksana, A. Kobayashi, A. Kinbara, J. Vac. Sci. Technol. A **10**, 1479 (1992)
71. Y. Guo, X.-W. Zhang, W.-H. Weng, G.-R. Han, Thin Solid Films **515**, 7117 (2007)
72. J.A. Gamboa, D.M. Pasquevich, J. Am. Ceram. Soc. **75**, 2934 (1992)
73. R.D. Shannon, J.A. Pask, J. Am. Ceram. Soc. **148**, 391 (1965)
74. M. Batzill, E.H. Morales, U. Diebold, Phys. Rev. Lett. **96**, 26103 (2006)
75. V. Schwartz, D.R. Mullins, W. Yan, B. Chen, S. Dai, S.H. Overbury, J. Phys. Chem. B **108**, 15782 (2004)
76. K. Yokota, K. Nakamura, Y. Yano, F. Miyashita, Surf. Coat. Technol. **158–159**, 573 (2002)
77. M. Takeuchi, Phys. Stat. Solidi (a) **55**, 653 (1979)